

# Theoretical investigation, empirical analysis and simulation of the growth pattern of traffic oscillations in the Euler coordinates

Junfang Tian<sup>1</sup>, Martin Treiber<sup>2</sup>, Rui Jiang<sup>3\*</sup>, Xiaopeng Li<sup>4\*</sup>, Bin Jia<sup>3</sup>, Ziyou Gao<sup>3</sup>

<sup>1</sup>*Institute of Systems Engineering, College of Management and Economics, Tianjin University, Tianjin 300072, China*

<sup>2</sup>*Institute for Transport & Economics, Technische Universität Dresden, Würzburger Str. 35, D-01062 Dresden, Germany*

<sup>3</sup>*MOE Key Laboratory for Urban Transportation Complex Systems Theory and Technology, Beijing Jiaotong University, Beijing 100044, China*

<sup>4</sup>*Department of Civil and Environmental Engineering, University of South Florida, FL 33620, USA*

The formation and development of oscillations is one of the most important phenomena in traffic flow. In recent studies, it was observed that traffic oscillations grow in a concave way along a vehicle platoon described in the Lagrangian specification. Since stationary bottlenecks are more intuitively described in the Eulerian framework, this paper investigates whether the concave growth pattern of traffic oscillations in the Lagrangian coordinates can be transferred to the Euler coordinates (i.e. the concave increase in standard deviation is no longer measured across the vehicle indices but as a function of the road location). To this end, we theoretically unify these two ways of measuring oscillations by revealing their mapping relationship. We show that the growth pattern measured in the Lagrangian coordinates can be transferred to the Euler coordinates without much quantitative distortion. To test this proposition, we analyze the NGSIM data, which shows that oscillations indeed grow in the concave way along the road. This validates our theoretical analysis. Finally, simulation of several microscopic and macroscopic models is performed. It is shown that in traditional models assuming a unique speed-spacing (or speed-density) relation, speed standard deviation initially increases in a convex way and then transits into concave growth pattern along the road. However, if a stochastic speed-spacing (or speed-density) relation is assumed in the models, then speed standard deviation increases in a concave way along the road. The simulation results further validate the theoretical analysis.

**Key words:** traffic oscillation; concave growth pattern; car following behavior; Euler coordinates

## 1. Introduction

Driving in smooth traffic flow makes passengers comfortable, saves fuel consumption and emissions and mitigates rear crash risks. Unfortunately, traffic flow is usually not smooth. Traffic oscillations have been observed frequently, in particular in congested traffic flow. A recent Japanese experiment ([Sugiyama et al., 2008](#))

---

\*Corresponding authors.

Email address: jftian@tju.edu.cn, martin@mtreiber.de, jiangrui@bjtu.edu.cn, xiaopengli@usf.edu

verified that when the density exceeds a threshold, traffic flow is always unstable. Traffic oscillations emerge and finally develop into traffic jam.

For over half a century, it is believed that the growth of oscillations is due to the linear instability of traffic steady state (see e.g., [Helbing, 2001](#); [Nagatani, 2002](#); [Nagel et al. 2003](#); [Wilson and Ward, 2011](#); [Treiber and Kesting, 2013](#)). [Li and Ouyang \(2011\)](#) and [Li et al. \(2012, 2014\)](#) showed with both theoretical and empirical results that nonlinear driving behavior may contribute to concave growth of traffic oscillations at least after oscillation amplitude becomes significant. Recently [Jiang et al. \(2014, 2015, 2017\)](#) conducted experimental studies of car following behavior on the open road section. The leading vehicle was asked to move with constant speed to simulate moving bottleneck. The formation and development of oscillations have been observed. It has been found that standard deviations of speed increase in a concave way along the platoon. Later, [Tian, et al. \(2016\)](#) investigated the propagation of traffic oscillations in the NGSIM vehicle trajectories. It has been found that traffic oscillations measured from empirical data also grow in a concave way highly consistent with the car following model predictions.

Simulation was performed ([Jiang et al., 2014, 2015](#)) using traditional car-following models based on the fundamental assumption that there is a unique relationship between traffic speed and vehicle spacing under steady state conditions, including the General Motor models (GMs, [Chandler et al., 1958](#); [Gazis et al. 1961](#); [Edie, 1961](#)), Gipps' Model ([Gipps, 1981](#)), Optimal Velocity Model (OVM, [Bando et al., 1995](#)), Full Velocity Difference Model (FVDM, [Jiang et al., 2001](#)), and Intelligent Driver Model (IDM, [Treiber et al., 2000](#)). Simulation results of these models run against the experimental finding since the standard deviation initially increases in a convex way in the unstable density range. It was shown that by removing the fundamental assumption and allowing the traffic state to span a two-dimensional region in velocity-spacing plane, the growth pattern of disturbances would change and become consistent with that observed in the experiment qualitatively or even quantitatively. In particular, the two-dimensional Intelligent Driver Model (2D-IDM) considering variable desired time gap can fit the experimental results quantitatively.

The importance of the concave growth of traffic oscillations lies in that it indicates that the instability mechanism of traditional models is questionable. In traditional models, the unstable traffic flow is generated due to linear instability of the steady state solution. In contrast, based on the experimental results, [Jiang et al. \(2017\)](#) argued that the traffic flow instability comes from the cumulative effect of stochastic factors, see also [Treiber and Kesting \(2017\)](#), [Laval et al. \(2014\)](#). As proved by [Li et al. \(2014\)](#), the linear instability in a nonlinear Newell model leads to initial convex growth of oscillations. We further demonstrate that small disturbances increase in a convex way in the initial stage in the traditional models assuming a unique relationship between speed and density ([Tian et al., 2016](#)), which was not consistent with the observed concave growth pattern.

Moving bottlenecks are more intuitively described in the Lagrangian specification co-moving with the bottleneck while stationary bottlenecks are better described in the Eulerian specification. Naturally, the question

arises whether the concave growth pattern within a vehicle platoon in the Lagrangian coordinates can be transferred to the settings of a fixed bottleneck in the Euler coordinates where the concave increase in speed standard deviation is no longer measured across the vehicle indices but along the road longitudinal location.

To address this issue, this paper reveals the relation between the propagation patterns of traffic oscillations upstream of moving and stationary bottlenecks. Firstly, we theoretically unify these two measures of oscillations in different coordinate systems by revealing their mapping relationship and demonstrate that the growth pattern measured in the Lagrangian coordinates can be transferred to the Euler coordinates without much quantitative distortion. Next, we performed an empirical study on the growth pattern of disturbances in NGSIM data, which showed that oscillations do grow in a concave way along the road. This validates the theoretical analysis. Finally, we carried out simulations with several microscopic and macroscopic models. It is found that in traditional models assuming a unique speed-spacing (or speed-density) relation, speed standard deviation initially increases in a convex way and then transits into concave growth pattern along the road. However, if a stochastic speed-spacing (or speed-density) relation<sup>†</sup> is assumed in the models, then speed standard deviation increases in a concave way along the road. The simulation results further validate the theoretical analysis.

The rest of this paper is organized as follows. Section 2 theoretically investigates the relation of oscillation growth pattern between Euler and Lagrangian coordinates. Section 3 analyzes the oscillation growth pattern along the road in empirical data. Section 4 performs simulation studies of the oscillation growth pattern along the road, and Section 5 concludes the paper.

## 2. Theoretical investigation

The investigated oscillation growth in the Euler coordinates can be essentially related to that in the Lagrangian coordinates characterized in earlier studies (Tian, et al. 2016). This section will theoretically unify these two measures of oscillations in different coordinate systems by revealing their mapping relationship. Specifically, we will compare temporal averages along single trajectories (Lagrangian view) with spatiotemporal averages considering all trajectories in a rectangular spatiotemporal region centered around a certain location (Eulerian view).

---

<sup>†</sup> One parameter of the relation changes with time stochastically, so that the state of traffic flow dynamically span a two-dimensional region on the speed-spacing (or speed-density) plane.

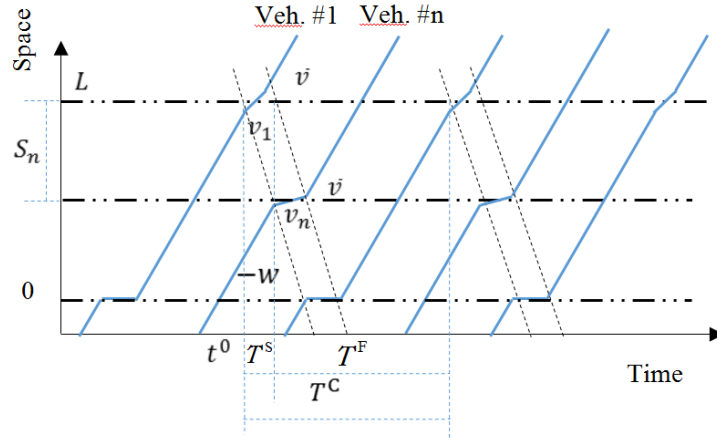


Figure 1. Schematic model of oscillations along trajectories.

Figure 1 presents a schematic model of oscillations along trajectories that approximates the basic periodic patterns. Basically, we assume that along the time horizon, trajectories repeat oscillation patterns with period  $T^C$ . Consider a highway segment between a downstream location  $L$  (near a bottleneck where the oscillation initiates) and an upstream location  $0$  and a typical period starting at  $t^0$ . We index the lead vehicle that initiates oscillation during this period with Vehicle 1, and increase the vehicle index from downstream to upstream. Now, we assume that the oscillation propagates backward along a shockwave at a constant velocity  $-w$  and the upstream vehicles follow a similar pattern with gradually amplified oscillations. We investigate the spatiotemporal region of trajectories between the shock wave that starts this period and the one that ends it. We call the region of slow trajectory segments the slow band and the region of cruising trajectories the cruise band. Along the propagation direction, the slow-moving speed  $v_n$  for Vehicle  $n$  in the slow band decreases with the vehicle index, while the cruising speed  $\hat{v}$  in the cruise band is independent of the vehicle index. Let  $s_n$  denote the average spacing between vehicles  $n-1$  and  $n$  (including the vehicle length) during the slow phase of the oscillation. Then, with simple geometry, we can calculate the distance of vehicle  $n$ 's position from location  $L$  at the beginning of the slow phase, denoted by  $S_n$ , as follows:

$$S_n := \sum_{n'=2}^n \frac{w s_{n'}}{v_{n'-1} + w}. \quad (1)$$

Furthermore, the slow band reaches Vehicle  $n$  at time  $t_n^0$ , which is given by

$$t_n^0 := t^0 + \frac{S_n}{w} = t^0 + \sum_{n'=2}^n \frac{s_{n'}}{v_{n'-1} + w}. \quad (2)$$

Note that the Euler speed distribution at location  $L - S_n$  during period  $[t_n^0, t_n^0 + T^C]$  is related to that of the Lagrangian speed measurements of vehicle  $n$  during this trajectory band in the following way. While the Euler measurements at location  $L - S_n$  stay at a speed close to  $v_n$  during  $[t_n^0, t_n^0 + T^S]$  and stay at  $\hat{v}$  during  $[t_n^0 + T^S, t_n^0 + T^C]$ , the Lagrangian speed measurements of vehicle  $n$  shall be at  $v_n$  during time  $[t_n^0, t_n^0 + t_n^S]$  and stay at  $\hat{v}$  during  $[t_n^0 + t_n^S, t_n^0 + t_n^C]$  where

$$t_n^C := t_n^S + t_n^F, t_n^S := \frac{T^S w}{w + v_n}, t_n^F := \frac{T^F w}{w + \hat{v}}. \quad (3)$$

This yields vehicle  $n$ 's average speed

$$\bar{v}_n^L := \frac{v_n t_n^S}{t_n^C} + \frac{\dot{v} t_n^F}{t_n^C},$$

and its Lagrangian speed STD is

$$\sigma_n^L := \sqrt{(v_n - \bar{v}_n^L)^2 t_n^S/t_n^C + (\dot{v} - \bar{v}_n^L)^2 t_n^F/t_n^C}. \quad (4)$$

This can be interpreted as a weighted operation of speeds  $v_n$  and  $\dot{v}$  with weights  $t_n^S/t_n^C$  and  $t_n^F/t_n^C$ , respectively.

In the Euler case, we examine the speed STD calculated from all trajectories in a fixed region (small ‘‘lattice cell’’)  $S_n$  during an oscillation cycle  $[t_n^0, t_n^0 + T^C]$ . Based on the conservation law, the vehicle density in the slow moving band  $[t_n^0, t_n^0 + T^S]$  (where vehicles cross location  $S_n$  at speed close to  $v_n$ ), denoted by  $\rho_n^S$ , and the vehicle density in the cruise band  $[t_n^0 + T^S, t_n^0 + T^C]$ , denoted by  $\rho_n^F$ , satisfy the following simple relationship:

$$\frac{\rho_n^S}{\rho_n^F} = \frac{w + \dot{v}}{w + v_n}. \quad (5)$$

Since the average vehicle number in the lattice cell is proportional to the density, the free and congested states are not only weighted with the corresponding Eulerian time intervals but also with the densities. Therefore, the average speed is given by

$$\bar{v}_{S_n}^E := v_n \frac{T^S \rho_n^S}{T^S \rho_n^S + T^F \rho_n^F} + \dot{v} \frac{T^F \rho_n^F}{T^S \rho_n^S + T^F \rho_n^F}.$$

With this, similar to Equation (4), the Euler speed STD detected at location  $S_n$ , denoted by  $\sigma_n^E$ , shall be a weighted

operation of speeds  $v_n$  and  $\dot{v}$  with weights  $\frac{T^S \rho_n^S}{T^S \rho_n^S + T^F \rho_n^F}$  and  $\frac{T^F \rho_n^F}{T^S \rho_n^S + T^F \rho_n^F}$ , respectively:

$$\sigma_{S_n}^E := \sqrt{(v_n - \bar{v}_{S_n}^E)^2 \frac{T^S \rho_n^S}{T^S \rho_n^S + T^F \rho_n^F} + (\dot{v} - \bar{v}_{S_n}^E)^2 \frac{T^F \rho_n^F}{T^S \rho_n^S + T^F \rho_n^F}}. \quad (6)$$

Note that with Equations (3) and (5), it is easy to see that  $\frac{T^S \rho_n^S}{T^S \rho_n^S + T^F \rho_n^F} = t_n^S/t_n^C$  and  $\frac{T^F \rho_n^F}{T^S \rho_n^S + T^F \rho_n^F} = t_n^F/t_n^C$ . Remarkably, this shows that the Euler speed STD are equivalent to the Lagrangian speed STD measures along individual vehicle trajectories:

$$\bar{v}_n^L = \bar{v}_{S_n}^E, \sigma_n^L = \sigma_{S_n}^E. \quad (7)$$

With this, if we are given Lagrangian STDs  $\sigma_n^L$  where  $\sigma_n^L$  is the STD for Vehicle  $n$ , then the corresponding Euler STDs  $\sigma_S^E$  where  $\sigma_S^E$  is the STD at location  $L - S$  can be estimated in the following way. First use equation (1) to obtain  $n$  such that  $S \in [S_{n-1}, S_n]$ . Then we can simply obtain  $\sigma_S^E$  as an interpolation of  $\sigma_n^L$  and  $\sigma_{n-1}^L$ . On the other hand, if we are given Euler STDs  $\{\sigma_{S^i}^E\}$ , then the corresponding Lagrangian STDs  $\sigma_n^L$  can be estimated in the similar way. Given a vehicle  $n$ , again find the corresponding distances  $S^{i-1}$  and  $S^i$  such that  $S_n \in [S^{i-1}, S^i]$ . Then we can interpolate  $\sigma_{S^i}^E$  and  $\sigma_{S^{i-1}}^E$  to obtain the  $\sigma_n^L$ . With this simplified relationship, we can see that the concavity growth of Lagrangian data implies that of Euler data, and vice versa.

### 3. Empirical data analysis

We analyze the US-101 trajectory data in the Next Generation Simulation data sets (NGSIM, 2006), which were collected on a 640 m segment on the south-bound direction of US-101 (Hollywood Freeway) in the vicinity of Lankershim Avenue in Los Angeles, California on June 15th, 2005. The data collected were from 07:50 a.m. to 08:35 a.m. Figure 2 provides a schematic illustration of the location for the vehicle trajectory datasets. There are five main lanes throughout the section, and an auxiliary lane directly connecting the on- and off-ramps.

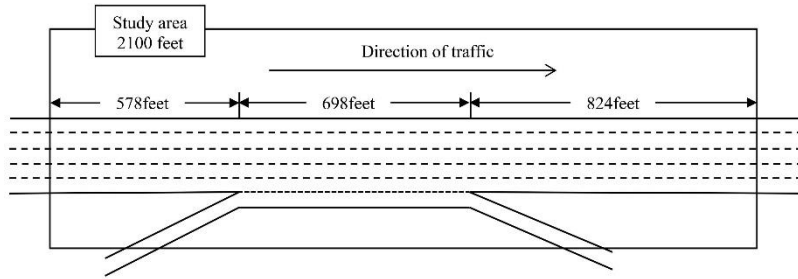


Figure 2. The sketch of US-101 study area.

We analyze the oscillations on the leftmost lane. To measure the oscillations along the road in a spatiotemporal way according to Section 2, we divide the study area (0 to 600 m) into 30 lattices of length 20 m, with the entrance of the road segment being the first lattice and the exit being the last lattice. As illustrated in Figure 3, we calculate the STDs and the means of the speeds along all trajectories in each lattice during the time interval  $[0, 770]$  s. Since the trajectories in the time interval  $[770, 1000]$ s involve jams propagating from the downstream section of the investigated area, they are excluded for the analysis. Figure 4(a) shows the means of the speeds. It indicates that the origin of the oscillations should be in the 18<sup>th</sup> lattice, since the mean speeds downstream of this location show a dramatically increasing trend compared with that upstream of this location. Figure 4(b) shows the standard deviations from the first lattice to the 18th lattice. The standard deviations of the speed increase in a concave way along the road. The result thus validates our theoretical analysis.

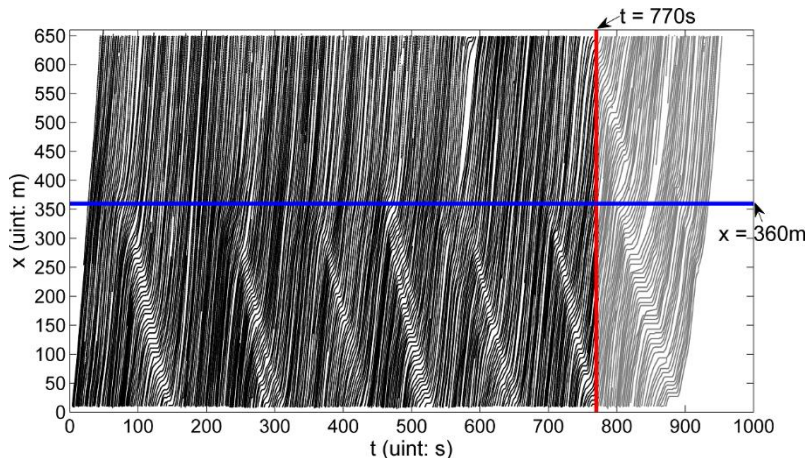


Figure 3. The NGSIM trajectories during the time interval 07:50am-08:05am from the leftmost lane.

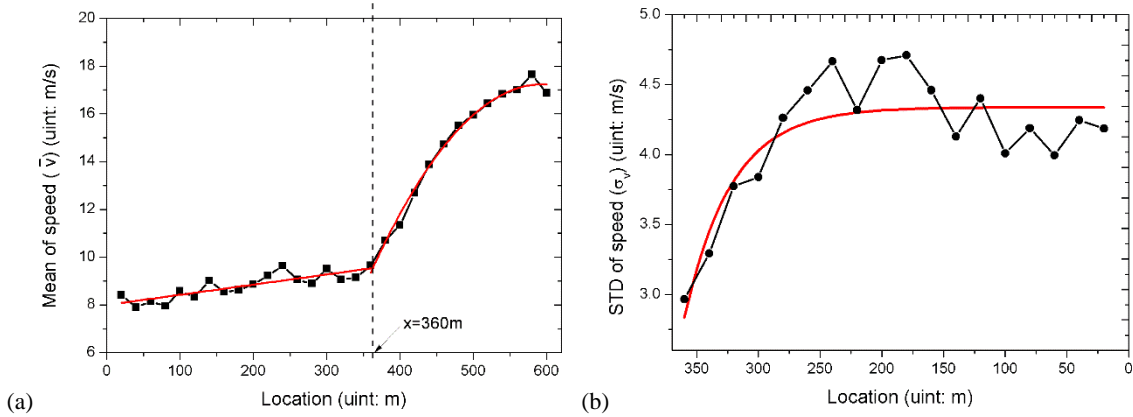


Figure 4. The mean and standard deviation (STD) of speed at each lattice, in which the red line is the fitted curve.

## 4. Simulations

This section carries out simulations of some microscopic and macroscopic models, i.e. the IDM, 2D-IDM, the speed gradient model (SGM, Jiang et al., 2002) and the 2D-SGM proposed below. The microscopic IDM and macroscopic SGM both assume unique speed-spacing and speed-density relations. In contrast, the microscopic 2D-IDM and macroscopic 2D-SGM assume the stochastic speed-spacing relations and speed-density relations, in which one parameter of the relation changes with time stochastically, respectively. In the latter two models, the traffic state can span the two-dimensional region in the corresponding planes. A speed limit bottleneck is implemented to examine the growth pattern of traffic oscillations.

For the microscopic models, the speed limit bottleneck is set as follows. The road length is set to 640 m and there is a speed limit region located at [360, 400] m. When vehicles enter this zone, their speed cannot exceed  $v_{lim}$  (i.e., if  $v > v_{lim}$ , then we set  $v = v_{lim}$ ). Note that the maximum speed does not change in this zone. We measure the standard deviation of speed in the Euler coordinate the same way as in Section 3. For macroscopic models, the road is classified into 32 lattices and the length of each lattice is  $\Delta x = 20m$ . There is a speed limit region located at the lattices 19 and 20, i.e. from 360 to 400 m, where the speed limit is  $v_{lim}$ . The initial density on all lattice is 0.03veh/m. Similar to the microscopic setting, if the speed  $u > v_{lim}$ , then we set  $u = v_{lim}$ . Here  $u$  is macroscopic speed in the lattice.

### 4.1 Simulations with models assuming the unique speed-spacing or speed-density relation

#### 4.1.1 The IDM

The IDM (Treiber et al., 2000) assumes that the acceleration  $a_n$  of vehicle  $n$  is given by a function of its speed  $v_n$ , the spacing  $d_n(t) = x_{n+1}(t) - x_n(t) - L_{veh}$  to the leading vehicle  $n+1$ , where  $x_n$  is location of vehicle  $n$  and  $L_{veh}$  is the length of the vehicle. The relative speed  $\Delta v_n(t) = v_{n+1}(t) - v_n(t)$  is the leading speed relative to the follower.

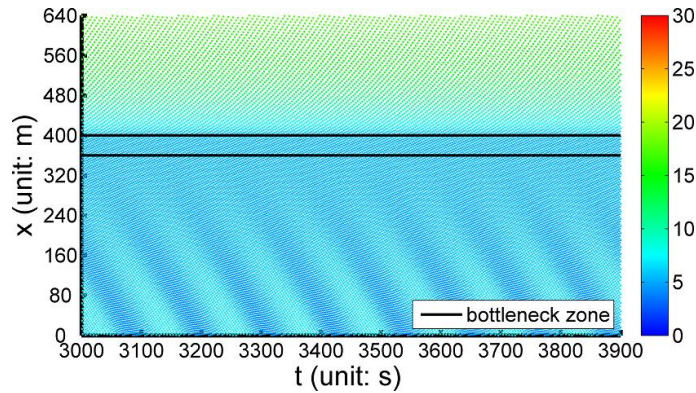
$$a_n(t) = a_{\max} \left( 1 - \left( \frac{v_n(t)}{v_{\max}} \right)^4 - \left( \frac{d_n^{\text{desired}}(t)}{d_n(t)} \right)^2 \right) \quad (8)$$

$$d_n^{\text{desired}}(t) = \max \left( v_n(t)T - \frac{v_n(t)\Delta v_n(t)}{2\sqrt{a_{\max}b}}, 0 \right) + d_0 \quad (9)$$

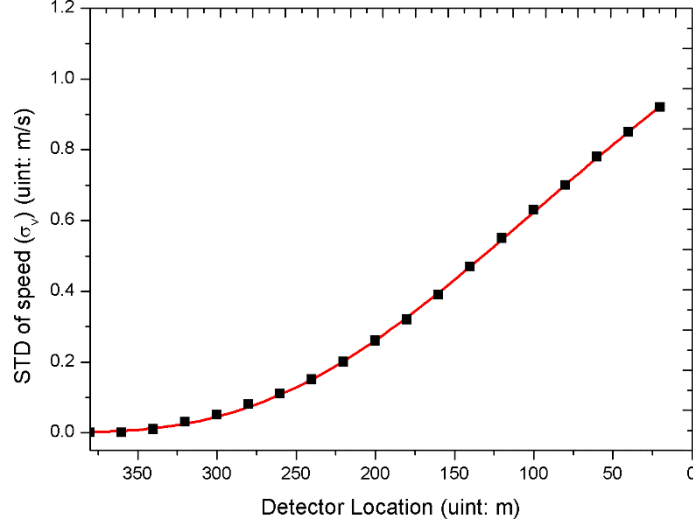
where  $v_{\max}$  is the maximum velocity,  $a_{\max}$  is the maximum acceleration,  $b$  is the comfortable deceleration,  $d_0$  is the jam gap,  $T$  is the desired time gap, and  $d_0$  is the minimum gap in jams.

Figure 5 shows that the macroscopic features of the formation and evolution of oscillations look similar to that in NGSIM data. In order to identify growth pattern of the oscillations, Figure 6 gives the standard deviation at the location from 0 to 360 m. It can be seen that the standard deviations of the speed initially increase in a convex way and then increase in the concave way along the road.

It is known that along a platoon, the speed standard deviation of vehicles initially increases in a convex way and then transits into concave growth in the IDM. The simulation thus again validates the theoretical analysis that the concave/convex growth measured in the Lagrangian coordinates can be transferred to the Euler coordinates.



**Figure 5.** The speed spatiotemporal diagram of the IDM. In the simulation, the parameters are set as:  $v_{\max}=30$  m/s,  $a_{\max}=0.73$  m/s<sup>2</sup>,  $b=1.67$  m/s<sup>2</sup>,  $d_0=1$  m,  $T=1.6$  s,  $L_{\text{veh}}=5$  m.  $v_{\text{lim}}=20$  km/h.



**Figure 6.** The standard deviation (STD) of speed of IDM at each detector, in which the red line is the fitted curve.

#### 4.1.2 The SGM

In the SGM proposed by Jiang et al. (2002), the speed gradient term has replaced the density gradient term in the equation of motion to overcome the wrong way travel problem pointed out by Daganzo (1995). The equations of SGM are as follows,

$$\frac{\partial \rho}{\partial t} + \frac{\partial(\rho u)}{\partial x} = 0 \quad (10)$$

$$\frac{\partial u}{\partial t} + u \frac{\partial u}{\partial x} = c_0 \frac{\partial u}{\partial x} + \frac{u_e - u}{\tau} \quad (11)$$

where  $\rho = \rho(x, t)$  and  $u = u(x, t)$  are the density and speed at position  $x$  and time  $t$ .  $c_0$  is the propagation speed of small disturbance,  $\tau$  is relaxation time,  $u_e = u_e(\rho)$  is the equilibrium speed-density relationship. We adopt the speed-density relationship proposed by Kerner and Konhäuser (1993).

$$u_e(\rho) = v_{max} \left( \frac{1}{1 + \exp\left(\frac{\rho / \rho_{max} - 0.25}{0.06}\right)} - 3.72 \times 10^{-6} \right) \quad (12)$$

where  $\rho_{max}$  is the maximum density. The SGM equations are discretized as follows (Jiang et al., 2002).

$$\rho_j^{n+1} = \rho_j^n + \frac{\Delta t}{\Delta x} (\rho_{j-1}^n u_j^n - \rho_j^n u_{j+1}^n) \quad (13)$$

$$u_j^{n+1} = \begin{cases} u_j^n - \frac{\Delta t}{\Delta x} (u_j^n - c_0)(u_{j+1}^n - u_j^n) + \frac{\Delta t}{T} (u_e(\rho_j^n) - u_j^n): & \text{if } u_j^n \leq c_0 \\ u_j^n - \frac{\Delta t}{\Delta x} (u_j^n - c_0)(u_j^n - u_{j-1}^n) + \frac{\Delta t}{T} (u_e(\rho_j^n) - u_j^n): & \text{if } u_j^n > c_0 \end{cases} \quad (14)$$

where the index  $j$  represents the road section and the index  $n$  represents time step;  $\Delta x$  and  $\Delta t$  are the sizes of space step and time step, respectively.

Figure 7 is the spatiotemporal diagram of SGM, which shows that macroscopic features of the formation and evolution of oscillations also look similar to that in the NGSIM data. However, as shown in Fig.8, in the SGM, the standard deviations of the speed also exhibit an initially convex growth pattern as in the IDM.

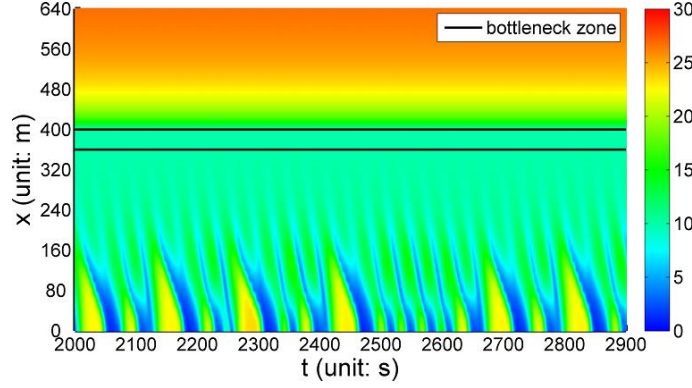


**Figure 7.** The speed spatiotemporal diagram of the SGM. In the simulation, the parameters are set as:  $v_{\max}=30$  m/s,  $c_0=11$  m/s,  $\rho_{\max} = 0.14$ veh/km,  $\tau = 5$  s,  $\Delta x = 20$  m,  $\Delta t = 0.02$  s and  $v_{\text{lim}} = 10$  m/s.

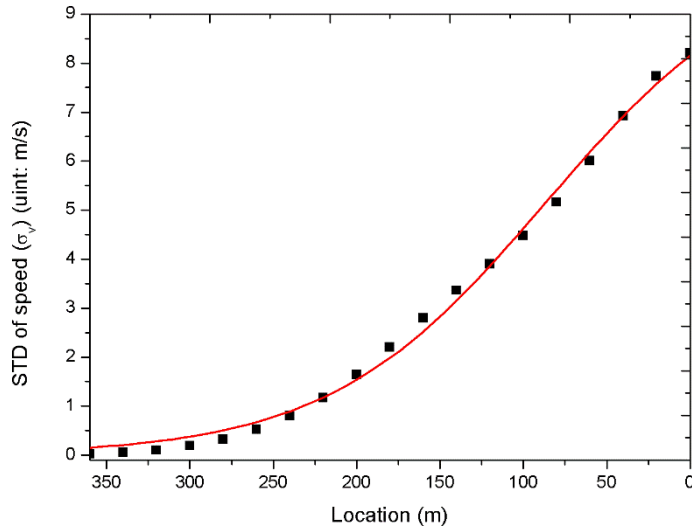


**Figure 8.** The standard deviation (STD) of speed of SGM.

#### 4.2 Simulations with models assuming the stochastic speed-spacing or speed-density relation

##### 4.2.1 The 2D-IDM

In contrast to the IDM where  $T$  is a constant parameter, the 2D-IDM proposed by Jiang et al. (2014) assumes that the desired time gap  $T$  is a stochastic quantity changing its value in each simulation step  $\Delta t = 0.1$  s as follows:

$$T(t + \Delta t) = \begin{cases} T_1 + rT_2 & \text{with probability } p, \\ T(t) & \text{otherwise.} \end{cases} \quad (15)$$

where  $r$  is the uniformly distributed random number between 0 and 1, the parameters  $T_1$  and  $T_1 + T_2$  indicating the

range of the time gap variations give rise to the two-dimensional speed-spacing states. Figure 9(a) shows the speed-spacing relation corresponding to  $T_1$  and  $T_1 + T_2$ , respectively.

Figure 10 and 11 are the simulation results of 2D-IDM, which show that the standard deviations of the speed increase in the concave way along the road, which further validates the theoretical analysis, because the speed standard deviation of vehicles increases in a concave way along a platoon in the 2D-IDM.

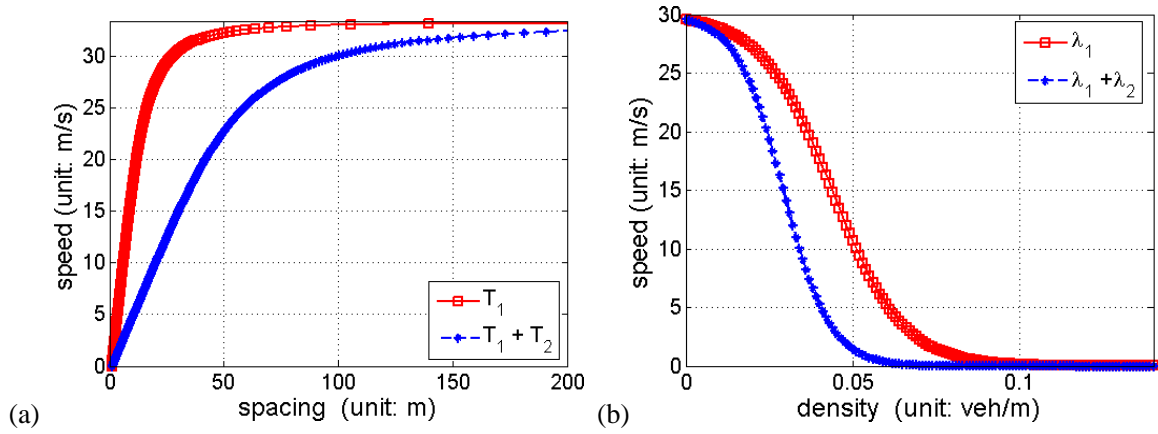


**Figure 9.** The range of speed-spacing relation of 2D-IDM (a) and the range of speed-density relation of 2D-SGM (b).

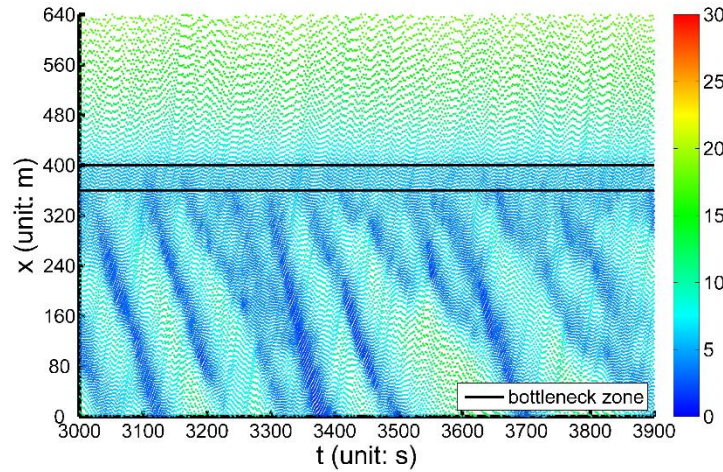


**Figure 10.** The spatiotemporal diagram of 2D-IDM. In the simulation, the parameters are set as:  $v_{\max}=30$  m/s,  $a_{\max}=0.73$  m/s<sup>2</sup>,  $b=1.67$  m/s<sup>2</sup>,  $d_0=1$  m,  $T_1=0.5$  s,  $T_2=1.4$  s,  $p=0.01$  and  $L_{\text{veh}}=5$  m,  $v_{\text{lim}}=20$  km/h.

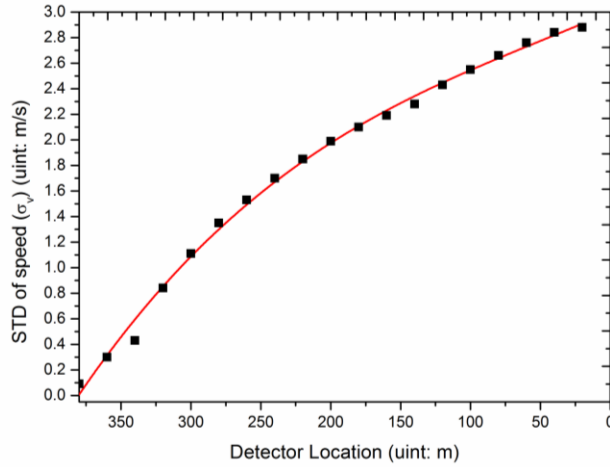


**Figure 11.** The standard deviation (STD) of speed of 2D-IDM at each detector, in which the red line is the fitted curve.

#### 4.2.2 The 2D-SGM

In the 2D-SGM, we have revised the speed-density relation of Kerner and Konhäuser (1993) as follows.

$$u_e(\rho) = v_{max} \left( \frac{1}{1 + \exp\left(\frac{\lambda(t)\rho / \rho_{max} - 0.25}{0.06}\right)} - 3.72 \times 10^{-6} \right) \quad (16)$$

where  $\lambda$  is a stochastic variable changing its value in each simulation step  $\Delta t$  as follows:

$$\lambda(t + \Delta t) = \begin{cases} \lambda_1 + r\lambda_2 & \text{with probability } p, \\ \lambda(t) & \text{otherwise.} \end{cases} \quad (17)$$

where  $r$  is a uniformly distributed random number between 0 and 1. The parameters  $\lambda_1$  and  $\lambda_1 + \lambda_2$  indicates the lower and upper bounds of the two-dimensional speed-density relation. Fig.9(b) shows the speed-density relation corresponding to  $\lambda_1$  and  $\lambda_1 + \lambda_2$ , respectively.

Figure 12 and 13 show the simulation results of 2D-SGM, in which the standard deviations of the speed grow in the concave way as in 2D-IDM.

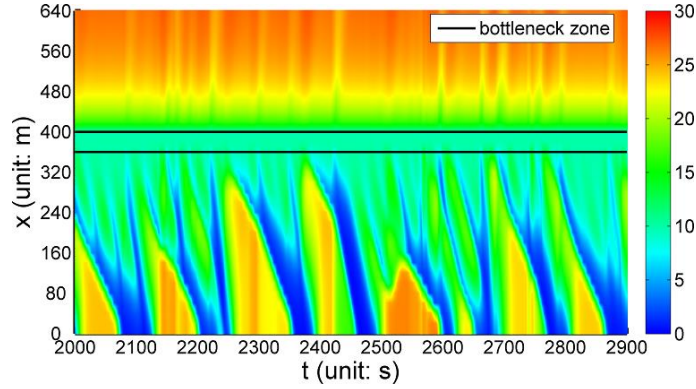


**Figure 12.** The spatiotemporal diagram of 2D-SGM. In the simulation,  $\lambda_1 = 0.8$ ,  $\lambda_2 = 0.4$ ,  $p = 0.002$ , and  $v_{lim} = 10$  m/s. Other parameters are the same as that of SGM.

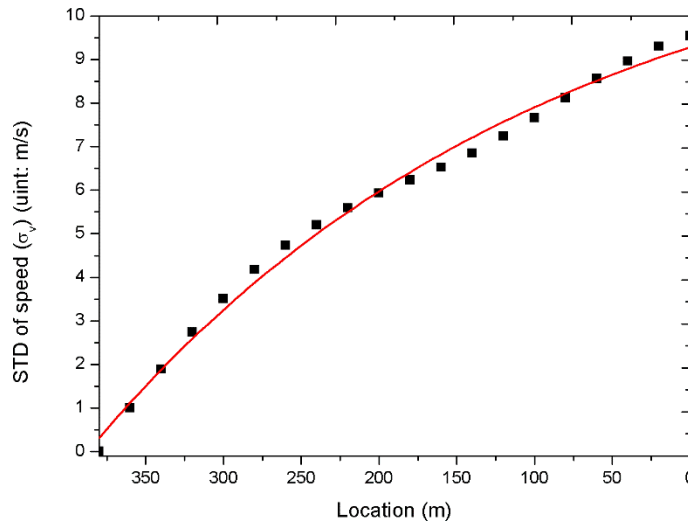


**Figure 13.** The standard deviation (STD) of speed of 2D-SGM, in which the red line is the fitted curve.

## 5. Conclusion

Propagation and growth of traffic oscillations play an important role in traffic flow dynamics. However, due to lack of high-precision trajectory data, the propagation mechanism of traffic oscillations is still unclear. While it is traditionally believed that growth of oscillations is due to the linear instability of traffic steady state, recent efforts (Jiang et al., 2014, 2015, 2017; Laval et al., 2014; Treiber and Kesting, 2017) indicate that stochastic factors lead to the growth of oscillations. This is because experimental and empirical data revealed that oscillations grow in a concave way along the platoon, while traditional models reproduce an initial convex growth of oscillations.

In previous studies (Jiang et al., 2014, 2015, 2017; Tian et al., 2016), the growth of oscillations is measured in the Lagrangian view. However, stationary bottlenecks are better described in the Eulerian framework. The

theoretical analysis in this paper shows that the concave growth pattern measured in the Lagrangian coordinates can be transferred to the Euler coordinates without much quantitative distortion. The empirical study on the oscillation growth in the NGSIM data validates the theoretical analysis qualitatively. Finally, simulation of several microscopic and macroscopic models shows that in traditional models, speed standard deviation initially increases in a convex way and then transits into concave growth pattern along the road. However, if a stochastic speed-spacing (or speed-density) relation is assumed in the models, then speed standard deviation increases in a concave way along the road. This further validates the theoretical analysis. Our study sheds further light the evolution mechanism of traffic oscillations.

We would like to mention that in the NGSIM data, the exact origin of the concerned oscillations is still not clear. For example, Chen et al. (2012) simulated the oscillations by introducing rubberneck effect, while Laval et al. (2014) introduced an uphill bottleneck. Moreover, in the NGSSIM data, the speed standard deviation has reached  $3.0 \text{ m/s}^2$  just upstream of the bottleneck. Therefore, the initial growth pattern of traffic oscillation is still unknown (In our simulation, we implement the speed limit bottleneck. As a result, the initial growth pattern is identified). Therefore, in the future work, more empirical and experimental data are needed to study the quantitative relation between bottleneck type, strength and the growth pattern of oscillations in the Euler coordinates.

## Acknowledgements

The authors wish to thank NGSIM for supplying the empirical data used in this article. JFT was supported by the National Natural Science Foundation of China (Grant No. 71771168, 71431005). RJ was supported by the Natural Science Foundation of China (Grant Nos. 71621001, 71631002 and 71371175). XL was supported by the US National Science Foundation through Grant CMMI# 1453949.

## Reference

- Bando, M., Hasebe, K., Nakayama, A., Shibata, A., Sugiyama, Y., 1995. Dynamical model of traffic congestion and numerical simulation. *Physical Review E* 51(2), 1035-1042. Chandler, R. E., Herman, R., Montroll, E. W., 1958. Traffic dynamics: studies in car following. *Operations research*, 6(2), 165-184.
- Chen, D., Laval, J., Zheng, Z., Ahn, S., 2012. A behavioral car-following model that captures traffic oscillations. *Transportation research part B: methodological*, 46(6), 744-761.
- Edie, L. C., 1961. Car-following and steady-state theory for noncongested traffic. *Operations Research* 9(1), 66-76.
- Gazis, D. C., Herman, R., Rothery, R. W., 1961. Nonlinear follow-the-leader models of traffic flow. *Operations Research* 9(4), 545-567.
- Gipps, P. G., 1981. A behavioural car-following model for computer simulation. *Transportation Research Part B: Methodological*, 15(2), 105-111.
- Helbing, D., 2001. Traffic and related self-driven many-particle systems. *Reviews of modern physics*, 73(4), 1067.
- Jiang, R., Wu, Q., Zhu, Z., 2001. Full velocity difference model for a car-following theory. *Physical Review E*, 64(1), 017101.
- Jiang, R., Hu, M. B., Zhang, H. M., Gao, Z.-Y., Jia, B., Wu, Q. S., Wang, B., Yang, M., 2014. Traffic experiment reveals the nature of car-following. *PloS one* 9(4), e94351.
- Jiang, R., Hu, M. B., Zhang, H. M., Gao, Z.-Y., Jia, B., Wu, Q. S., 2015, On some experimental features of car-following behavior and how to model them. *Transportation Research Part B: Methodological* 80, 338-354.

- Jiang, R., Jin, C. J., Zhang, H. M., Huang, Y. X., Tian, J. F., Wang, W., Hu, M. B., Wang, H., Jia, B., 2017. Experimental and empirical investigations of traffic flow instability. *ISTTT 22; Transportation Research Part C* (in press).
- Kerner, B. S., Konhäuser, P., 1993. Cluster effect in initially homogeneous traffic flow. *Physical Review E*, 48(4), R2335.
- Kerner, B. S., 1998. Experimental Features of Self-Organization in Traffic Flow. *Physical Review Letters* 81:3797-3800.
- Laval, J. A., Toth, C. S., & Zhou, Y., 2014. A parsimonious model for the formation of oscillations in car-following models. *Transportation Research Part B: Methodological*, 70, 228-238.
- Li, X., Ouyang, Y., 2011. Characterization of traffic oscillation propagation under nonlinear car-following laws. *Transportation research part B: methodological*, 45(9), 1346-1361.
- Li, X., Wang, X., Ouyang, Y., 2012. Prediction and field validation of traffic oscillation propagation under nonlinear car-following laws. *Transportation Research Part B*, 46(3), 409-423.
- Li, X., Cui, J., An, S., Parsafard, M., 2014. Stop-and-go traffic analysis: theoretical properties, environmental impacts and oscillation mitigation. *Transportation Research Part B*, 70, 319–339
- Mauch, M., J. Cassidy, M., 2002. Freeway traffic oscillations: observations and predictions. *Transportation and Traffic Theory in the 21st Century: Proceedings of the 15th International Symposium on Transportation and Traffic Theory*, 653-673.
- Nagatani, T., 2002. The physics of traffic jams. *Reports on Progress in Physics* 65 (9), 1331.
- Nagel, K., Wagner, P., Woesler, R. 2003. Still flowing: Approaches to traffic flow and traffic jam modeling. *Operations research*, 51(5), 681-710.
- Sugiyama, Y., Fukui, M., Kikuchi, M., Hasebe, K., Nakayama, A., Nishinari, K., Nishinari, K., Tadaki, S. C., Yukawa, S., 2008. Traffic jams without bottlenecks—experimental evidence for the physical mechanism of the formation of a jam. *New journal of physics*, 10(3), 033001.
- Tian, J., Jiang, R., Jia, B., Gao, Z., Ma, S., 2016. Empirical analysis and simulation of the concave growth pattern of traffic oscillations. *Transportation Research Part B: Methodological*, 93, 338-354.
- Treiber, M. Kesting, A., 2013. *Traffic flow dynamics: data, models and simulation*. Springer.
- Treiber, M. Kesting, A., 2017. The Intelligent Driver Model with stochasticity - New insights into traffic flow oscillations. *ISTTT 22; Transportation Research Part B* (in press).
- Treiber, M., Hennecke, A., and Helbing, D., 2000. Congested traffic states in empirical observations and microscopic simulations. *Physical Review E* 62(2), 1805.
- Wilson, R. E., Ward, J. A., 2011. Car-following models: fifty years of linear stability analysis—a mathematical perspective. *Transportation Planning and Technology*, 34(1), 3-18.